A New and Simple Meshless LBIE-RBF Numerical Scheme in Linear Elasticity

E.J. Sellountos [1]**, D. Polyzos**[2] **and S.N. Atluri**[3]**,**

Abstract: A new meshless Local Boundary Integral Equation (LBIE) method for solving two-dimensional elastostatic problems is proposed. Randomly distributed points without any connectivity requirement cover the analyzed domain and Local Radial Basis Functions (LRBFs) are employed for the meshless interpolation of displacements. For each point a circular support domain is centered and a local integral representation for displacements is considered. At the local circular boundaries tractions are eliminated with the aid of companion solution, while at the intersections between the local domains and the global boundary displacements and tractions are treated as independent variables avoiding thus derivatives of LRBFs. Stresses are evaluated with high accuracy and without derivatives of LRBFs via a LBIE valid for stresses. All the integrations are performed quickly and economically and in a way that renders the extension of the method to three-dimensional problems straightforward. Six representative numerical examples that demonstrate the accuracy of the proposed methodology are provided.

1   Introduction

After the pioneering work of [Zhu, Zhang, and Atluri (1998)], the Local Boundary Integral Equation (LBIE) method has been established as an excellent alternative to the Boundary Element Method (BEM), since it circumvents problems associated with mesh and fully populated matrices as well as with volume integrals when the fundamental solution of the problem is not available. It is characterized as being

---

[1] Department of Mathematics and CEMAT, Instituto Superior Técnico, Technical University of Lisbon, Lisbon, Portugal.

[2] Department of Mechanical Engineering and Aeronautics, University of Patras, Greece, Institute of Chemical Engineering and High Temperature Process ICETH-FORTH, Rio, Greece.

[3] University of California, Irvine, Center for Aerospace Research & Education, Irvine, CA 92612, USA.

"truly meshless" since properly distributed nodal points, without any connectivity requirement, covering the domain of interest as well as the surrounding global boundary are employed instead of any boundary or finite element discretization. No background cells are required for the numerical evaluation of the involved integrals and all fields are interpolated with the aid of meshless Moving Least Squares (MLS) approximation scheme or via Local Radial Basis Functions (LRBFs) properly defined for the support domain of each point. The local nature of the sub-domains leads to a final linear system of equations the coefficient matrix of which is sparse and not fully populated.

In the framework of linear elasticity, the first LBIE methodology is due to [Atluri, Sladek, Sladek, and Zhu (2000)]. Their work can be considered as a direct extension of the work of [Zhu, Zhang, and Atluri (1998)] to elastostatic problems. After that work many papers dealing with meshless LBIE solutions of linear elastic problems have appeared in the literature. Representative are those of [Sladek, Sladek, and Keer (2000)], [Sladek, Sladek, and Keer (2003)], [Sladek, Sladek, and Atluri (2002)], [Atluri, Han, and Shen (2003)], [Han and Atluri (2003a)], [Sellountos and Polyzos (2003)], [Sellountos and Polyzos (2005b)], [Sellountos and Polyzos (2005a)], [Sellountos, Vavourakis, and Polyzos (2005)], [Bodin, Ma, Xin, and Krishnaswami (2006)], [Vavourakis, Sellountos, and Polyzos (2006)], [Zhu, Zhang, and Wang (2007)], [Vavourakis and Polyzos (2008)][Vavourakis and Polyzos (2007)], [Vavourakis (2008)][Vavourakis (2009)], [Vavourakis, Protopappas, Fotiadis, and Polyzos (2009)], [Sladek, Sladek, Solek, Tan, and Zhang (2009)], [Sellountos, Sequeira, and Polyzos (2009)][Sellountos, Sequeira, and Polyzos (2010)], [Sladek and Sladek (2010)] and [Wen and Aliabadi (2012)] while a comprehensive presentation of meshless LBIE methods can be found in the books of [Atluri and Shen (2002)] and [Atluri (2004)].

After the work of [Atluri, Sladek, Sladek, and Zhu (2000)], [Sellountos and Polyzos (2003)] proposed a new LBIE method for solving frequency domain elastodynamic problems. The main differences between the two methodologies were that [Sellountos and Polyzos (2003)] treated boundary displacements and tractions as independent variables avoiding thus the use of derivatives of MLS approximation functions and moreover made use of a relatively uniform distribution of nodal points so that the MLS interpolation scheme to posses delta property [Gosz and Liu (1996)] and the boundary conditions to be imposed directly on the nodal displacements and tractions. However, although accurate, the requirement of using uniform distribution of nodal points confines the method to structures with regular only shapes. In order to avoid that requirement [Sellountos, Vavourakis, and Polyzos (2005)] and [Vavourakis and Polyzos (2007)] proposed a new LBIE/MLS methodology where at each nodal point both singular and hypersingular LBIEs were employed for the

LBIE representation of displacement and traction fields. The problem here is that the need of treating displacements and stresses as independent variables throughout the analyzed domain increases drastically the degrees of freedom of the problem, thus making the method prohibitive for large- scale analysis. Very recently [Sellountos, Sequeira, and Polyzos (2009)] presented the LBIE method of [Sellountos and Polyzos (2003)] with the difference of using an efficient Local Radial Basis Functions (LRBF) scheme ([Sellountos and Sequeira (2008a)][Sellountos and Sequeira (2008b)]) instead of MLS approximation functions for the interpolation of displacements. Although that technique overcomes most of the drawbacks appearing in [Sellountos and Polyzos (2003)], [Sellountos, Vavourakis, and Polyzos (2005)] and [Vavourakis and Polyzos (2007)], it utilizes the complicated integration techniques of [Sellountos and Polyzos (2003)], which actually prevents the extension of the method to three dimensions. Finally, [Sellountos, Sequeira, and Polyzos (2010)] proposed a LBIE/RBF technique, completely different to previous ones and very promising for solving three- dimensional problems. However, its requirement of using background Finite Element Method type cells confines drastically the meshless nature of the method.

The present paper demonstrates a new LBIE/RBF method for the solution of elastostatic problems. Its philosophy is very simple and its extension to three dimensions straightforward. It employs the classical LBIEs for displacements and stresses as it is explained in the next section. All the integrations at local boundaries are performed with the aid of simple BEM- techniques while all the fields are interpolated via the efficient RBF interpolation scheme of [Sellountos and Sequeira (2008a)][Sellountos and Sequeira (2008b)] presented in the section after next. RBFs satisfy delta property and hence boundary conditions are automatically taken into account. Moreover the inverse matrix utilized in the final RBF interpolation depends only on the relative placement of the nearby nodal points [Atluri and Shen (2002)] and thus it is computed only once. Both characteristics are very important and contribute significantly to the efficiency of the method. The numerical implementation of the method is very simple and it is illustrated in detail in section 4. The main advantages of the method are its simplicity and the evaluation of displacements, boundary tractions and stresses without the need of RBF derivatives. Six benchmark problems are provided in section 5 as a demonstration of the accuracy achieved by the proposed LBIE/RBF method.

2 Local integral equations for displacements and stresses

Consider a two-dimensional linear and isotropic elastic domain Ω surrounded by a surface Γ. Assuming zero body forces, the displacement vector u_i defined at any
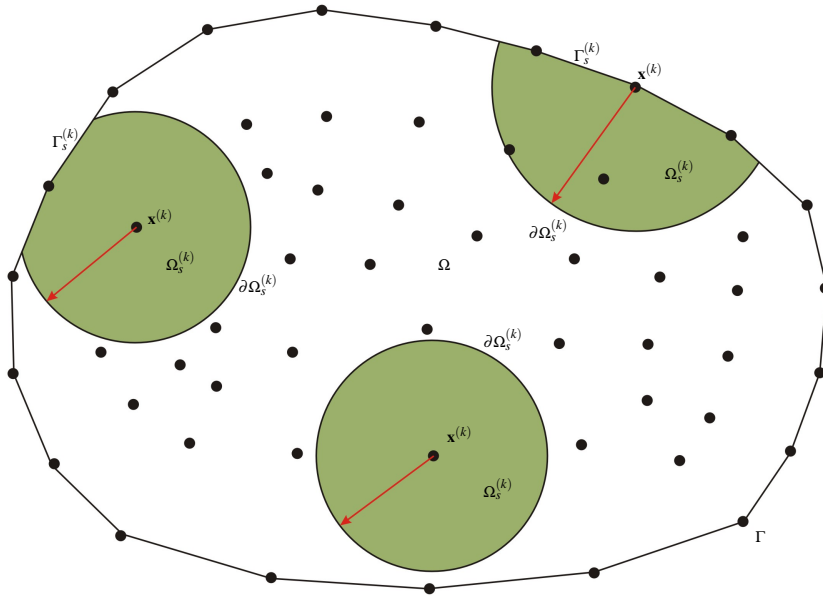
Figure 1: Local domains and local boundaries used for the LBIE representation of displacements at point $\mathbf{x}^{(k)}$.

point $\mathbf{x}$ of the body satisfies the Navier-Cauchy partial differential equation:

$$\mu\partial_j^2 u_i(\mathbf{x}) + (\lambda + \mu)\,\partial_i\partial_j u_j(\mathbf{x}) = 0 \tag{1}$$

where λ, μ represent the Lam's constants and ∂_i denotes differentiation with respect to Cartesian coordinate x_i. The boundary conditions are assumed to be

$$u_i(\mathbf{x}) = \bar{u}_i(\mathbf{x}), \mathbf{x} \in \Gamma_u$$
$$t_i(\mathbf{x}) = \bar{t}_i(\mathbf{x}), \mathbf{x} \in \Gamma_t \tag{2}$$

with t_i denoting traction vector, $\bar{u}_i, \bar{t}_i$ prescribed vectors and $\Gamma_u \cup \Gamma_t \equiv \Gamma$. The elastic domain Ω and the boundary Γ are covered by randomly distributed points without any connectivity requirement. Any point $\mathbf{x}^{(k)}$ of the analyzed domain is considered to be the center of a local circular domain Ω_s (with boundary $\partial\Omega_s$) called support domain of $\mathbf{x}^{(k)}$ as it is illustrated in Fig. 1. Employing the elastostatic fundamental solution of Eq. 1 [Polyzos, Tsinopoulos, and Beskos (1998)] and applying Betti's reciprocal identity for displacement vector and fundamental solution, one obtains

the following LBIE for the support domain of any interior or boundary point $\mathbf{x}^{(k)}$

$$u_i\left(\mathbf{x}^{(k)}\right) + \int_{\partial\Omega_s} t_{ij}^*\left(\mathbf{x}^{(k)},\mathbf{y}\right) u_j(\mathbf{y}) \, d\Gamma_y = \int_{\partial\Omega_s} u_{ij}^*\left(\mathbf{x}^{(k)},\mathbf{y}\right) t_j(\mathbf{y}) \, d\Gamma_y \tag{3}$$

when the support domain is interior to Ω and

$$cu_i\left(\mathbf{x}^{(k)}\right) + \int_{\partial\Omega_s \cup \Gamma_s} t_{ij}^*\left(\mathbf{x}^{(k)},\mathbf{y}\right) u_j(\mathbf{y}) \, d\Gamma_y = \int_{\partial\Omega_s \cup \Gamma_s} u_{ij}^*\left(\mathbf{x}^{(k)},\mathbf{y}\right) t_j(\mathbf{y}) \, d\Gamma_y \tag{4}$$

when the support domain intersects the global boundary on $\Gamma_s \equiv \partial\Omega_s \cap \Gamma$. The coefficient c is equal to 1 for internal points and $1/2$ for points lying on the global boundary Γ with smooth tangent. In the present formulation, boundary points are imposed with the aid of a BEM mesh. At both sides of a corner, partially discontinuous boundary elements are considered. Thus the coefficient c is always equal to $1/2$ for any nodal point belonging to the global boundary Γ. Finally, u_{ij}^*, t_{ij}^* represent the fundamental displacement and traction tensors, respectively, given by [Polyzos, Tsinopoulos, and Beskos (1998)]

$$u_{ij}^* = \frac{1}{8\pi\mu(1-\nu)}\left[-(3-4\nu)\ln r\,\delta_{ij} + (\partial_i r)(\partial_j r)\right] \tag{5}$$

$$t_{ij}^* = \frac{1}{2\pi}\left[\frac{1-2\nu}{2(1-\nu)}\frac{1}{r}\left[(\partial_i r)\,n_j - (\partial_j r)\,n_i\right] - \frac{1-2\nu}{2(1-\nu)}\frac{1}{r}(\partial_m r)\,n_m\delta_{ij} - \right.$$
$$\left. \frac{1}{1-\nu}\frac{1}{r}\left[n_m(\partial_m r)(\partial_i r)(\partial_j r)\right]\right] \tag{6}$$

where $r = |\mathbf{y} - \mathbf{x}|$, $\mathbf{x}, \mathbf{y}$, represent the field and source point, respectively, δ_{ij} is Kronecker delta and n_i the unit vector being normal to the local boundary.

In order to get rid of tractions defined on $\partial\Omega_s$ the use of the companion solution u_{ij}^c is made [Atluri, Sladek, Sladek, and Zhu (2000)] and the LBIEs Eq. 3 and Eq. 4 obtain the form, respectively

$$u_i\left(\mathbf{x}^{(k)}\right) + \int_{\partial\Omega_s}\left[t_{ij}^*\left(\mathbf{x}^{(k)},\mathbf{y}\right) - t_{ij}^c\left(\mathbf{x}^{(k)},\mathbf{y}\right)\right] u_j(\mathbf{y}) \, d\Gamma_y = 0 \tag{7}$$

and

$$cu_i\left(\mathbf{x}^{(k)}\right) + \int_{\partial\Omega_s \cup \Gamma_s}\left[t_{ij}^*\left(\mathbf{x}^{(k)},\mathbf{y}\right) - t_{ij}^c\left(\mathbf{x}^{(k)},\mathbf{y}\right)\right] u_j(\mathbf{y}) \, d\Gamma_y =$$
$$\int_{\Gamma_s}\left[u_{ij}^*\left(\mathbf{x}^{(k)},\mathbf{y}\right) - u_{ij}^c\left(\mathbf{x}^{(k)},\mathbf{y}\right)\right] t_j(\mathbf{y}) \, d\Gamma_y \tag{8}$$

where

$$u_{ij}^c = \frac{1}{8\pi\mu(1-v)} \frac{r^2}{r_0^2} (\partial_i r)(\partial_j r) +$$
$$\frac{1}{8\pi\mu(1-v)} \left[\frac{5-4v}{2(3-4v)} \left(1 - \frac{r^2}{r_0^2}\right) - (3-4v)\ln r_0 \right] \delta_{ij} \tag{9}$$

$$t_{ij}^c = \frac{1}{4\pi(1-v)(3-4v)r_0^2} \left[3(\partial_i r)n_j - (\partial_j r)n_i - (\partial_m r)n_m \delta_{ij} \right] \tag{10}$$

and r_0 is the radius of the support domain Ω_s.

Eq. 7 and Eq. 8 represent the LBIE valid for any interior and boundary point, respectively, of the analyzed domain. Employing a methodology explained in [Sellountos, Vavourakis, and Polyzos (2005)], one can find the LBIE for stresses, i.e.

$$\sigma_{ik}\left(\mathbf{x}^{(k)}\right) + \int_{\partial\Omega_s} \left[S_{ikj}^*\left(\mathbf{x}^{(k)}, \mathbf{y}\right) - S_{ikj}^c\left(\mathbf{x}^{(k)}, \mathbf{y}\right) \right] u_j(\mathbf{y}) \, d\Gamma_y +$$
$$\int_{\Omega_s} F_{ikj}\left(\mathbf{x}^{(k)}, \mathbf{y}\right) u_j(\mathbf{y}) \, d\Omega_y = 0 \tag{11}$$

for interior support domains and

$$c\sigma_{ik}\left(\mathbf{x}^{(k)}\right) + \int_{\partial\Omega_s \cup \Gamma_s} \left[S_{ikj}^*\left(\mathbf{x}^{(k)}, \mathbf{y}\right) - S_{ikj}^c\left(\mathbf{x}^{(k)}, \mathbf{y}\right) \right] u_j(\mathbf{y}) \, d\Gamma_y +$$
$$\int_{\Omega_s} F_{ikj}\left(\mathbf{x}^{(k)}, \mathbf{y}\right) u_j(\mathbf{y}) \, d\Omega_y = \tag{12}$$
$$\int_{\Gamma_s} \left[V_{ikj}^*\left(\mathbf{x}^{(k)}, \mathbf{y}\right) - V_{ikj}^c\left(\mathbf{x}^{(k)}, \mathbf{y}\right) \right] t_j(\mathbf{y}) \, d\Gamma_y$$

for support domains that intersect the global boundary *S*. The kernels appearing in Eq. 11 and Eq. 12 have the form:

$$F_{ikj} = \frac{\mu}{2\pi} \left\{ 2 \left(\frac{dR}{dr} - \frac{R}{r} \right) (\partial_i r)(\partial_k r)(\partial_j r) + \right.$$
$$\left(\frac{R}{r} - \frac{dQ}{dr} \right) \left[(\partial_i r)\delta_{kj} + (\partial_k r)\delta_{ij} \right] - \tag{13}$$
$$\left. \left[\frac{2v}{1-2v} \left(\frac{dQ}{dr} - \frac{dR}{dr} - \frac{R}{r} \right) - \frac{2R}{r} \right] (\partial_j r)\delta_{ik} \right\}$$

where

$$
Q = \frac{2(3-4\nu)}{1-2\nu}A_2 - \frac{5-4\nu}{1-2\nu}B_2 - \frac{2(3-2\nu)}{1-2\nu}B_3 r
$$

$$
R = \frac{9-10\nu}{1-2\nu}B_3 r
$$

$$
A_2 = -\frac{3-4\nu}{8(1-\nu)}\frac{1}{r_0^2}, B_2 = -\frac{3}{4(1-\nu)}\frac{1}{r_0^2}, B_3 = \frac{1}{2(1-\nu)}\frac{1}{r_0^3}
$$

(14)

and

$$
V_{ikj} = \frac{1}{2\pi}\left\{2\left(\frac{dX^a}{dr}-\frac{X^a}{r}\right)(\partial_i r)(\partial_k r)(\partial_j r)+\right.
$$
$$
\left(\frac{X^a}{r}-\frac{d\Psi^a}{dr}\right)\left[(\partial_i r)\delta_{kj}+(\partial_k r)\delta_{ij}\right]-
$$
$$
\left.\left[\frac{2\nu}{1-2\nu}\left(\frac{d\Psi^a}{dr}-\frac{dX^a}{dr}-\frac{X^a}{r}\right)-\frac{2X^a}{r}\right](\partial_j r)\delta_{ik}\right\}
$$

(15)

$$
S_{ikj} = \frac{\mu}{2\pi}\left\{\beta_1\left[n_m(\partial_m r)\right](\partial_j r)\delta_{ik}+\beta_2\left[n_m(\partial_m r)\right]\left[(\partial_i r)\delta_{kj}+(\partial_k r)\delta_{ij}\right]-\right.
$$
$$
\beta_3\left[n_m(\partial_m r)\right](\partial_i r)(\partial_k r)(\partial_j r)+\beta_4\left[n_i\delta_{kj}+n_k\delta_{ij}\right]+
$$
$$
\left.\beta_1(\partial_i r)(\partial_k r)n_j+\beta_2\left[n_i(\partial_k r)(\partial_j r)+n_k(\partial_i r)(\partial_j r)\right]-\beta_5\delta_{ik}n_j\right\}
$$

(16)

$$
\beta_1 = 4\left(\frac{1}{r}\frac{dX^a}{dr}-\frac{2X^a}{r^2}\right)+\frac{4\nu}{1-2\nu}\left(\frac{d^2X^a}{dr^2}-\frac{d^2\Psi^a}{dr^2}+\frac{1}{r}\frac{d\Psi^a}{dr}-\frac{2X^a}{r^2}\right)
$$

$$
\beta_2 = -\frac{d^2\Psi^a}{dr^2}+\frac{1}{r}\frac{d\Psi^a}{dr}+\frac{3}{r}\frac{dX^a}{dr}-\frac{6X^a}{r^2}
$$

$$
\beta_3 = -4\left(\frac{d^2X^a}{dr^2}-\frac{5}{r}\frac{dX^a}{dr}+\frac{8X^a}{r^2}\right)
$$

(17)

$$
\beta_4 = 2\left(\frac{X^a}{r^2}-\frac{1}{r}\frac{d\Psi^a}{dr}\right)
$$

$$
\beta_5 = \left(\frac{2\nu}{1-2\nu}\right)^2\left(\frac{d^2\Psi^a}{dr^2}-\frac{d^2X^a}{dr^2}-\frac{2}{r}\frac{dX^a}{dr}+\frac{1}{r}\frac{d\Psi^a}{dr}\right)-
$$
$$
\frac{4X^a}{r^2}-\frac{8\nu}{1-2\nu}\left(\frac{1}{r}\frac{dX^a}{dr}-\frac{1}{r}\frac{d\Psi^a}{dr}+\frac{X^a}{r^2}\right)
$$

where the superscript (a) corresponds either to (*) for fundamental solution kernels

or to (c) for the companion ones, and

$$\Psi^* = -\frac{3-4\nu}{4(1-\nu)}\ln r, \quad X^* = -\frac{1}{4(1-\nu)}$$

$$\Psi^c = -\frac{3-4\nu}{8(1-\nu)}\frac{r^2}{r_0^2}, \quad X^c = \frac{1}{4(1-\nu)}\frac{r^2}{r_0^2}\left(2\frac{r}{r_0}-3\right) \tag{18}$$

It should be mentioned here that the LBIE of Eq. 11 is always regular, since the kernel F_{ikj} is regular with respect to $r = |\mathbf{y} - \mathbf{x}^{(k)}|$ and in the hypersingular kernel $S_{ikj}^*\left(\mathbf{x}^{(k)}, \mathbf{y}\right)$ the point of interest $\mathbf{x}^{(k)}$ does not coincide the integration point $\mathbf{y}$. However, this is not the case for LBIE of Eq. 12 where $\mathbf{x}^{(k)}$ meets the integration point $\mathbf{y}$ at the part of the global boundary Γ_s. An elegant way to avoid one the hypersigular nature of Eq. 12 is to utilize the non-hypersingular LBIE formulation described in detail in the works of [Okada, Rajiyah, and Atluri (1989a)], [Okada, Rajiyah, and Atluri (1989b)] and [Han and Atluri (2003b)], [Han and Atluri (2007)]. That could be the subject of a future work.

3   The Radial Basis Functions interpolation scheme

After the pioneering work of [Hardy (1990)], global RBFs have been extensively used in meshless and collocation numerical methods either as interpolation functions [Atluri (2004)] or for the transformation of volume integrals to surface ones in the Dual Reciprocity BEM (DRBEM) [Nardini and Brebbia (1982)] [Agnantiaris, Polyzos, and Beskos (1996)]. However, the use of globally supported RBFs requires the inversion of ill-conditioned dense matrices with obvious computational cost. Despite the significant progress, the use of globally supported RBFs leads to computationally expensive nonlocal formulations that confine their use to relatively small-scale problems. A solution to that problem is the use of compactly supported RBFs or Local RBFs (LRBFs). Considering local support domains for their definition, the implementation of LRBFs leads to sparse systems of equations with apparent gains. In the present work LRBFs based on multiquadric (MQ) functions are employed for the interpolation of displacements. Their positive definitiveness is accomplished with the use of an additional polynomial term together with a homogeneous constraint condition. That regulation in conjunction with the fact that no derivatives of LRBFs are required renders the present MQ-LRBFs interpolation scheme robust and efficient. It should be mentioned, however that the optimum size of the support domains is of crucial importance for the achieved accuracy of the proposed here LBIE methodology.

In the present section the RBF interpolation scheme employed in the present work is illustrated.

Consider an elastic domain Ω surrounded by a boundary Γ covered by arbitrarily distributed nodal points $\mathbf{x}^{(k)}, k = 1, 2, ... N$ as shown in Fig. 2. As in Fig. 1 each nodal point is considered as the centre of a small circular domain Ω_k of radius r_k called support domain of $\mathbf{x}^k$. All support domains of a group of adjacent nodal points that satisfy the condition

$$\left| \mathbf{x}^{(k)} - \mathbf{x}^{(j)} \right| < r_k + r_j$$

form a domain called domain of influence of point $\mathbf{x}^{(k)}$ (Fig. 2). The nodal points that contain in their support domain a point $\mathbf{x}$ form the domain of definition of point $\mathbf{x}$.

At any point $\mathbf{x}$ of Ω, the interpolation of the unknown dispacement component $u_\alpha(\mathbf{x}), \alpha = 1$ or 2 is accomplished by the relation

$$u_\alpha(\mathbf{x}) = \mathbf{B}^T(\mathbf{x}) \cdot \mathbf{a}^{(\alpha)} + \mathbf{P}^T(\mathbf{x}) \cdot \mathbf{b}^{(\alpha)}$$

or

$$u_\alpha(\mathbf{x}) = \begin{bmatrix} \mathbf{B}^T(\mathbf{x}) & \mathbf{P}^T(\mathbf{x}) \end{bmatrix} \cdot \begin{bmatrix} \mathbf{a}^{(\alpha)} \\ \mathbf{b}^{(\alpha)} \end{bmatrix} \tag{19}$$

where

$$\begin{aligned}
\mathbf{x} &= \begin{bmatrix} x_1 & x_2 \end{bmatrix}^T \\
\mathbf{a}^{(\alpha)} &= \begin{bmatrix} a_1^{(\alpha)} & a_2^{(\alpha)} & ... & a_n^{(\alpha)} \end{bmatrix}^T \\
\mathbf{b}^{(\alpha)} &= \begin{bmatrix} b_1^{(\alpha)} & b_2^{(\alpha)} & ... & b_m^{(\alpha)} \end{bmatrix}^T \\
\mathbf{B}(\mathbf{x}) &= \begin{bmatrix} W(\mathbf{x}, \mathbf{x}^{(1)}) & W(\mathbf{x}, \mathbf{x}^{(2)}) & ... & W(\mathbf{x}, \mathbf{x}^{(n)}) \end{bmatrix}^T \\
\mathbf{P}(\mathbf{x}) &= \begin{bmatrix} P_1(\mathbf{x}) & P_2(\mathbf{x}) & ... & P_m(\mathbf{x}) \end{bmatrix}^T
\end{aligned} \tag{20}$$

with n representing the total number of nodal points belonging to the domain of definition of point $\mathbf{x}$ and m the number of complete polynomials with $m < n$. The vectors $\mathbf{a}^{(\alpha)}$ and $\mathbf{b}^{(\alpha)}$ stand for unknown coefficient vectors that depend on the location of the nodal points belonging to the domain of definition of point $\mathbf{x}$. $\mathbf{P}(\mathbf{x})$ is a vector containing the monomial basis, i.e.

$$\begin{aligned}
\mathbf{P}(\mathbf{x}) &= \begin{bmatrix} 1 & x_1 & x_2 \end{bmatrix} \text{ for } m = 3 \\
\mathbf{P}(\mathbf{x}) &= \begin{bmatrix} 1 & x_1 & x_2 & x_1^2 & x_1 x_2 & x_2^2 \end{bmatrix} \text{ for } m = 6
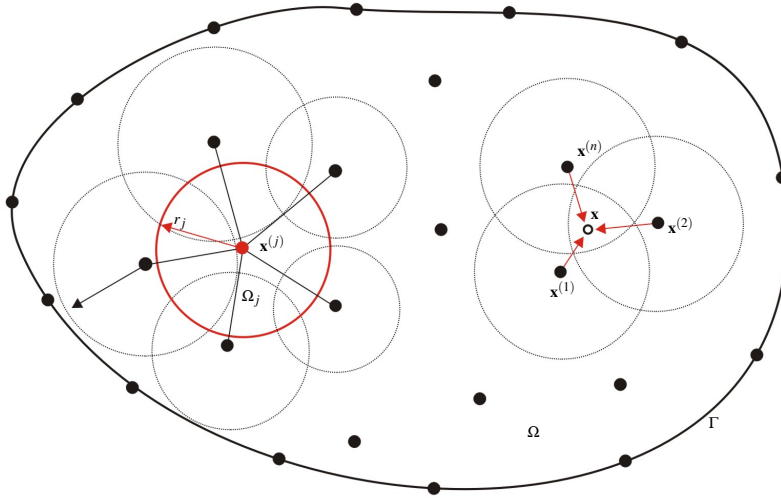\end{aligned} \tag{21}$$

Figure 2: Domain of influence of the point $\mathbf{x}^{(j)}$ and domain of definition of point $\mathbf{x}$.

and $W(\mathbf{x}, \mathbf{x}^{(n)})$ are RBFs defined in the present work as multiquadric LRBFs (MQ-LRBFs)

$$W(\mathbf{x}, \mathbf{x}^{(n)}) = \sqrt{(x_1 - x_1^{(n)})^2 + (x_2 - x_2^{(n)})^2 + C^2} \tag{22}$$

For the domain of definition of $\mathbf{x}$, C is a constant the value of which is taken as [Hardy (1990)]

$$C(\mathbf{x}) = 0.815 \frac{1}{n} \sum_{i=1}^{n} d_i \tag{23}$$

with d_i being the distance between every nodal point of the domain of definition of $\mathbf{x}$ and its closest nodal neighbor.

The definition of the unknown vectors $\mathbf{a}^{(\alpha)}$ and $\mathbf{b}^{(\alpha)}$ is accomplished by imposing and interpolation passing of Eq. 19 through all nodal points $\mathbf{x}^{(n)}$, i.e.

$$u_\alpha(\mathbf{x}^{(e)}) = \begin{bmatrix} \mathbf{B}^T(\mathbf{x}^{(e)}) & \mathbf{P}^T(\mathbf{x}^{(e)}) \end{bmatrix} \begin{bmatrix} \mathbf{a}^{(\alpha)} \\ \mathbf{b}^{(\alpha)} \end{bmatrix}, e = 1, 2, ..., n \tag{24}$$

and considering the extra system of algebraic equations [Wang and Liu (2002a)]

$$\sum_{e=1}^{n} P_l\left(x^{(e)}\right) \mathbf{a}_e^{(\alpha)}, l = 1, 2, ..., m. \tag{25}$$

Thus, the following system of equations is formed:

$$\begin{bmatrix} \mathbf{B}_0 & \mathbf{P}_0 \\ \mathbf{P}_0^T & \mathbf{0} \end{bmatrix} \begin{bmatrix} \mathbf{a}^{(\alpha)} \\ \mathbf{b}^{(\alpha)} \end{bmatrix} = \begin{bmatrix} \mathbf{u}_\alpha^{(e)} \\ \mathbf{0} \end{bmatrix} \tag{26}$$

where

$$\mathbf{B}_0 = \begin{bmatrix} W\left(\mathbf{x}^{(1)}, \mathbf{x}^{(1)}\right) & W\left(\mathbf{x}^{(1)}, \mathbf{x}^{(2)}\right) & \dots & W\left(\mathbf{x}^{(1)}, \mathbf{x}^{(n)}\right) \\ W\left(\mathbf{x}^{(2)}, \mathbf{x}^{(1)}\right) & W\left(\mathbf{x}^{(2)}, \mathbf{x}^{(2)}\right) & \dots & W\left(\mathbf{x}^{(2)}, \mathbf{x}^{(n)}\right) \\ \dots & \dots & \dots & \dots \\ W\left(\mathbf{x}^{(n)}, \mathbf{x}^{(1)}\right) & W\left(\mathbf{x}^{(n)}, \mathbf{x}^{(2)}\right) & \dots & W\left(\mathbf{x}^{(n)}, \mathbf{x}^{(n)}\right) \end{bmatrix} \tag{27}$$

$$\mathbf{P}_0 = \begin{bmatrix} P_1\left(\mathbf{x}^{(1)}\right) & P_2\left(\mathbf{x}^{(1)}\right) & \dots & P_m\left(\mathbf{x}^{(1)}\right) \\ P_1\left(\mathbf{x}^{(2)}\right) & P_2\left(\mathbf{x}^{(2)}\right) & \dots & P_m\left(\mathbf{x}^{(2)}\right) \\ \dots & \dots & \dots & \dots \\ P_1\left(\mathbf{x}^{(n)}\right) & P_2\left(\mathbf{x}^{(n)}\right) & \dots & P_m\left(\mathbf{x}^{(n)}\right) \end{bmatrix} \tag{28}$$

and

$$\mathbf{u}_\alpha^{(e)} = \begin{bmatrix} u_\alpha^{(1)} & u_\alpha^{(2)} & \dots & u_\alpha^{(n)}. \end{bmatrix}^T \tag{29}$$

In view of Eq. 26 the coefficient vector $\left[\mathbf{a}^{(\alpha)} \ \mathbf{b}^{(\alpha)}\right]^T$ is equal to

$$\begin{bmatrix} \mathbf{a}^{(\alpha)} \\ \mathbf{b}^{(\alpha)} \end{bmatrix} = \mathbf{A}^{-1} \begin{bmatrix} \mathbf{u}_\alpha^{(e)} \\ \mathbf{0} \end{bmatrix} \tag{30}$$

where $\mathbf{A}$ is the symmetric matrix

$$\mathbf{A} = \begin{bmatrix} \mathbf{B}_0 & \mathbf{P}_0 \\ \mathbf{P}_0^T & \mathbf{0} \end{bmatrix}. \tag{31}$$

Finally, the interpolation Eq. 19 obtains the form

$$u_\alpha(\mathbf{x}) = \begin{bmatrix} \mathbf{B}^T(\mathbf{x}) & \mathbf{P}^T(\mathbf{x}) \end{bmatrix} \cdot \mathbf{A}^{-1} \cdot \begin{bmatrix} \mathbf{u}_\alpha^{(e)} \\ \mathbf{0} \end{bmatrix} = \mathbf{R} \cdot \mathbf{u}_\alpha^{(e)} \tag{32}$$

where

$$\mathbf{R} = \begin{bmatrix} R^{(1)} & R^{(2)} & \dots & R^{(n)} \end{bmatrix}$$

$$R^{(e)} = \sum_{i=1}^{n} B_i(\mathbf{x}) A_{ie}^{-1} + \sum_{j=1}^{m} P_j(\mathbf{x}) A_{(n+j)e}^{-1} , \ e = 1, 2, ..., n \tag{33}$$

with A_{qr}^{-1} representing the (qr)-element of the matrix $\mathbf{A}^{-1}$.

More details on the local LRBFs one can find in the book of [Atluri (2004)] and in the representative works of [Wang and Liu (2002b)][Wang and Liu (2002a)], [Gilhooley, Xiao, Batra, McCarthy, and Gillespie (2008)] and [Bourantas, Skouras, Loukopoulos, and Nikiforidis (2010)].

4 Numerical implementation

In this section the numerical implementation of the proposed LBIE methodology is presented. Consider the elastic domain Ω surrounded by a boundary Γ, depicted in Fig. 1 and a set of arbitrarily distributed and without any connectivity requirement points, called nodal points, that cover the domain Ω. The global boundary Γ is represented by a group of points imposed by a boundary element mesh. The nodes of the boundary element mesh are considered also as nodal points of the problem.

As it has been already mentioned in section 2, for points $\mathbf{x}^{(k)}$ with non intersected by the global boundary support domains, the corresponding displacement vector $u_i\left(\mathbf{x}^{(k)}\right)$ admits a LBIE of the form

$$u_i\left(\mathbf{x}^{(k)}\right) + \int_{\partial\Omega_s} \left[t_{ij}^*\left(\mathbf{x}^{(k)}, \mathbf{y}\right) - t_{ij}^c\left(\mathbf{x}^{(k)}, \mathbf{y}\right) \right] u_j(\mathbf{y})\, dS_y = 0 \tag{34}$$

The key idea of the present LBIE methodology is that the local boundary $\partial\Omega_s$ of $\mathbf{x}^{(k)}$ is discretized into L quadratic line elements as it is shown in Fig. 3. Therefore Eq. 34 can be written as

$$u_i^{(k)} + \left(\sum_{e=1}^{L} \sum_{n=1}^{3} \int_{-1}^{1} \left[t_{ij}^* - t_{ij}^c \right] N_{jm} J\, d\xi \right) u_m^{en} = 0 \tag{35}$$

where N_{jm} are shape functions corresponding to quadratic elements, J is the Jacobian of the transformation from the global to the local coordinate system ξ and u_m^{en} represent displacements at the boundary element nodes. It should be noticed here that the boundary element nodes at the local boundary (shown as red points in Fig. 3) have not any relation with the initially considered nodal points.

In the sequel, each boundary element nodal displacement is interpolated via the RBF scheme illustrated in previous section, i.e.

$$u_i^{(k)} + \left(\sum_{e=1}^{L} \sum_{n=1}^{3} \int_{-1}^{1} \left[t_{ij}^* - t_{ij}^c \right] N_{jm} J\, d\xi \right) R_{ml} u_l^p = 0 \tag{36}$$
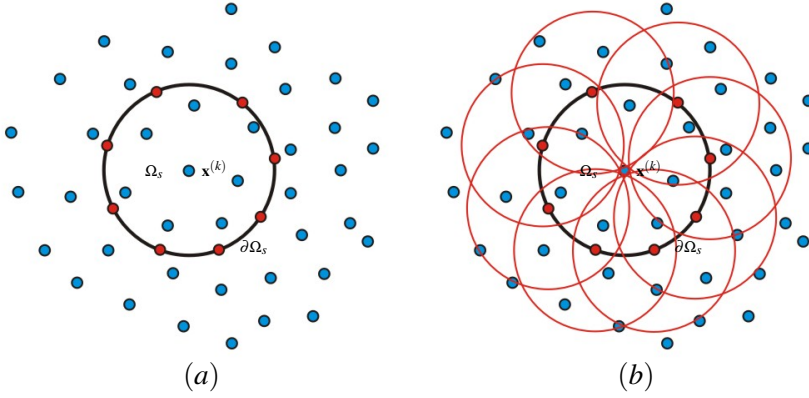
Figure 3: (a) The local boundary $\partial\Omega_s$ of point $\mathbf{x}^{(k)}$ discretized into quadratic boundary elements. The nodes of those elements are indicated by the red points. (b) The domain of influence of the nodal point $\mathbf{x}^{(k)}$ formed by all the RBF support domains of the boundary element nodes (red circles). The domain of influence defines the number of nodal points (blue points) involved in the LBIE of $\mathbf{x}^{(k)}$.

or in matrix form

$$\mathbf{H}^{(k)} \cdot \mathbf{u}^{(k)} = \mathbf{0} \tag{37}$$

where R_{ml} represents the RBF interpolation matrix with rows illustrated by relations Eq. 32 and Eq. 33, $u_i^{(p)}$ the nodal values of displacements involved in the support domains of all local boundary element nodes, shown in Fig. 3, and $\mathbf{u}^{(k)}$ a vector containing all displacement components of $u_i^{(p)}$.

For a boundary nodal point $\mathbf{x}^{(k)}$, the LBIE has the form of Eq. 8 for $c = 0.5$, i.e.

$$\frac{1}{2} u_i\left(\mathbf{x}^{(k)}\right) + \int_{\partial\Omega_s \cup \Gamma_s} \left[t_{ij}^*\left(\mathbf{x}^{(k)}, \mathbf{y}\right) - t_{ij}^c\left(\mathbf{x}^{(k)}, \mathbf{y}\right) \right] u_j\left(\mathbf{y}\right) dS_y =$$
$$\int_{\Gamma_s} \left[u_{ij}^*\left(\mathbf{x}^{(k)}, \mathbf{y}\right) - u_{ij}^c\left(\mathbf{x}^{(k)}, \mathbf{y}\right) \right] t_j\left(\mathbf{y}\right) dS_y \tag{38}$$

It should be mentioned here that at corners discontinuous boundary elements are utilized. Consequently the LBIE Eq. 38 is employed for all points at the global boundary of the analyzed domain. Following the previous procedure, the local boundary $\partial\Omega_s$ of $\mathbf{x}^{(k)}$ is discretized into K quadratic line elements, while the intersected boundary Γ_s is divided into M line quadratic elements, which are part of the
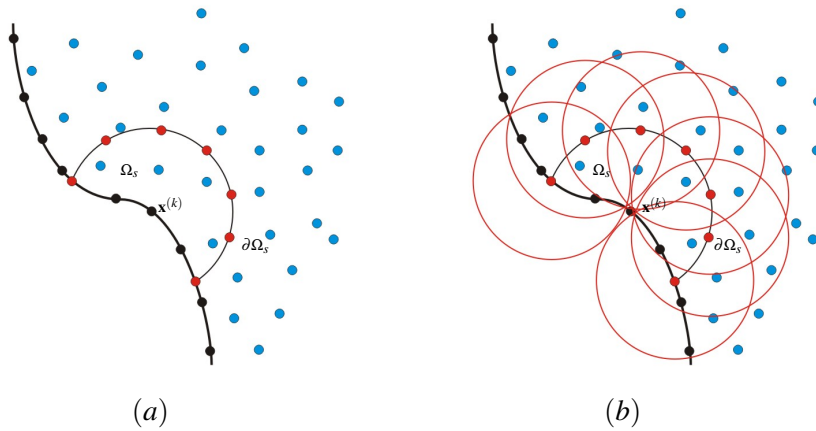
Figure 4: (a) The local boundary $\partial\Omega_s \cup \Gamma_s$ corresponding to boundary point $\mathbf{x}^{(k)}$ discretized into quadratic boundary elements. As in Fig. 3, red points represent the nodes utilized for the mesh of $\partial\Omega_s$. Black points indicate nodes corresponding to line quadratic elements used for the representation of the global boundary Γ. (b) The domain of influence of the boundary nodal point $\mathbf{x}^{(k)}$ formed by all the RBF support domains of the boundary element nodes (red circles).

boundary element mesh used for the representation of the global boundary Γ. Thus, displacements and tractions defined at Γ_s are interpolated as independed variables through quadratic line elements. Both boundary element nodes and nodal points are illustrated in Fig. 4. Splitting Eq. 38 into boundary elements one obtains

$$
\begin{aligned}
\frac{1}{2}u_i^{(k)} + \sum_{e=1}^{K}\sum_{n=1}^{3}\int_{-1}^{1}\left[t_{ij}^* - t_{ij}^c\right]N_{jm}J\,d\xi\,R_{ml}u_l^{(p)} + \\
\sum_{e=1}^{M}\sum_{n=1}^{3}\int_{-1}^{1}\left[t_{ij}^* - t_{ij}^c\right]N_{jm}J\,d\xi\,R_{ml}u_l^{(s)} = \\
\sum_{e=1}^{M}\sum_{n=1}^{3}\int_{-1}^{1}\left[u_{ij}^* - u_{ij}^c\right]N_{jm}J\,d\xi\,t_m^{(s)}
\end{aligned}
\tag{39}
$$

where $u_i^{(p)}$ stand for he nodal values of displacements involved in the support domains of all local boundary element nodes at $\partial\Omega_s$, while $u_l^{(s)}, t_l^{(s)}$ represent the boundary displacements and tractions, respectively, defined at the boundary element nodes of Γ_s. M_{ml} is boundary interpolation functions.

Applying the boundary conditions and rearranging, Eq. 39 is written in a matrix form as

$$\mathbf{H}^{(k)} \cdot \mathbf{u}^{(k)} + \mathbf{G}^{(k)} \cdot \mathbf{t}^{(k)} = \mathbf{b}^{(k)} \tag{40}$$

with the vectors $\mathbf{u}^{(k)}, \mathbf{t}^{(k)}$ containing all the unknown displacements and tractions, respectively, and $\mathbf{b}^{(k)}$ a vector consisting of all the displacements and tractions known by the boundary conditions.

It is apparent that the final vector equation corresponding to an internal nodal point the support domain of which intersects the global boundary, is similar to Eq. 40.

In view of Eq. 37 and Eq. 40, the following final system of algebraic equations is obtained

$$\mathbf{A} \cdot \mathbf{z} = \mathbf{b} \tag{41}$$

with the vector $\mathbf{z}$ comprising all the unknown nodal displacements and tractions, while the vector $\mathbf{b}$ contains prescribed components of vectors. This system can be solved easily and efficiently through a typical LU decomposition solver since, due to the local nature of the method, the matrix $\mathbf{A}$ is sparse and banded. As soon as all the nodal values of displacements and boundary tractions have been calculated, the stresses at any nodal point $\mathbf{x}^{(k)}$ can be evaluated through the LBIE Eq. 11 for internal points and LBIE Eq. 12 for boundary or nearly to the boundary nodal points. The evaluation of displacements, boundary tractions and stresses without using derivatives of the RBF interpolation functions is, among others, a significant advantage of the proposed method.

5 Numerical examples

5.1 *Rectangular plate in tension*

The first problem concerns the tension of the $1m$x$1m$ rectangular plate depicted in Fig. 5(a). The Young modulus and the Poisson ratio have been considered to be equal to $E = 100000N/m^2$ and $v = 0.25$, respectively, while the tensional traction at the free side of the plate is $P = 1N/m^2$. Totally 13 nodal points, shown in Fig. 5(b), have been used for the solution of the problem and the radius of the support domains has been selected to be the same for all nodes and equal to 1.132m. The vertical displacements across the line AB of the plate (Fig. 5(a)) have been evaluated with the proposed here LBIE methodology and they compared to analytical ones [Saad (2005)] in Fig. 6. As it is observed the obtained results are in excellent agreement with the analytical solution of the problem.
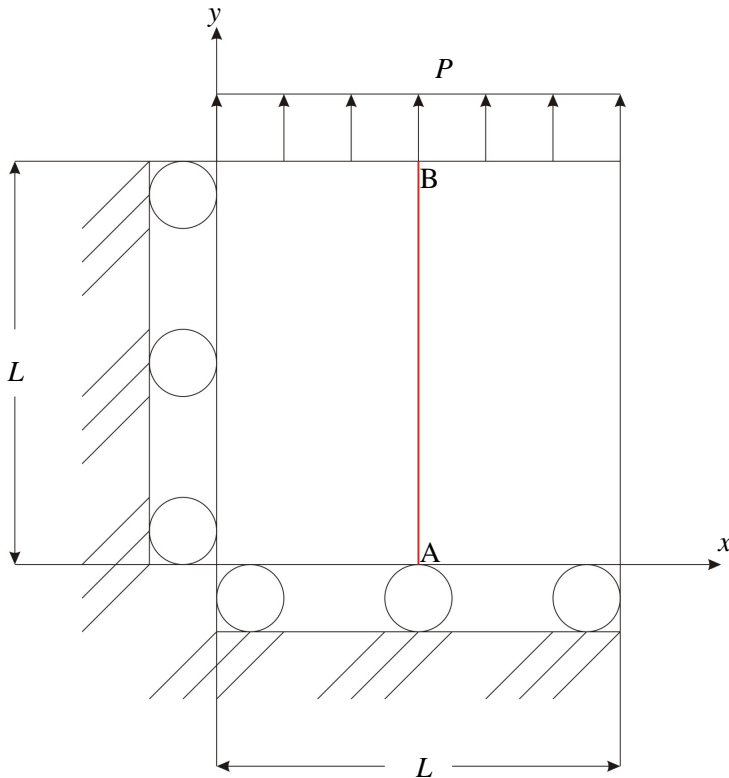
(a)
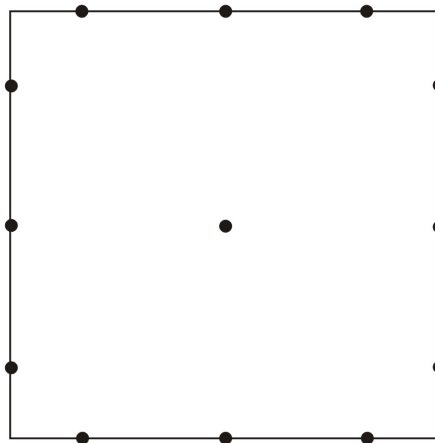
(b)

Figure 5: (a) Tension of a square plate of L=1m. (b) Distribution of the used nodal points.
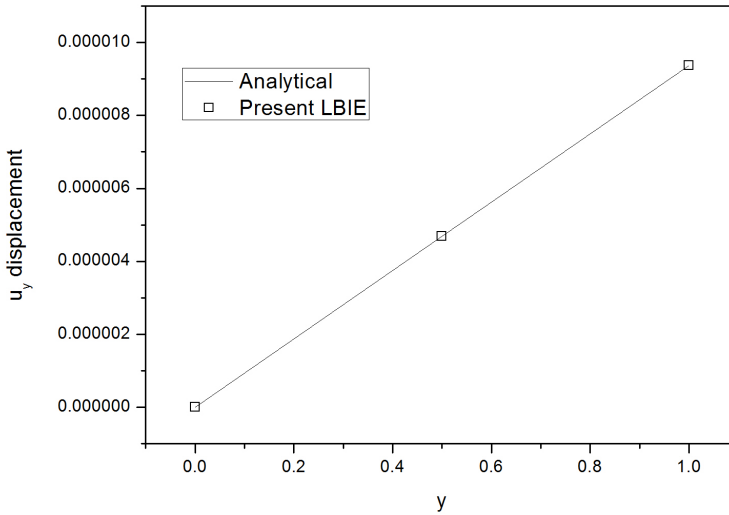
Figure 6: Vertical displacements across the line AB depicted in Fig. 5(a).

5.2 Cantilever beam in bending

The beam of Fig. 7(a) with $E = 100000 N/m^2$ and $v = 0.25$ is subjected to a vertical traction load $P = 1N/m^2$. Utilizing 209 nodal points (Fig. 7(b)) with the same support domain of radius $0.566m$, the vertical displacements along the line AB, the axial tractions at the clamped side of the beam and the stresses sxx, sxy at the cross-section CD have been evaluated and compared to the corresponding analytical solutions [Selvadurai (2000)] in Fig. 8, Fig. 9, Fig. 10 and Fig. 11, respectively. All comparisons show a very good agreement between numerical and analytical results.

5.3 Cylinder subjected to an internal pressure

Consider a long cylindrical shell with inner and outer radii $r_i = 1m$ and $r_o = 2m$, respectively, subjected to an internal uniform pressure $P = 1N/m^2$. The material properties of the cylinder are the same as in the previous two numerical examples and the analytical solution of the problem is provided in [Polyzos, Tsinopoulos, and Beskos (1998)]. Due to the symmetry of the problem only one quarter of the cylinder needs to be considered (Fig. 12(a)), while a distribution of 179 nodal
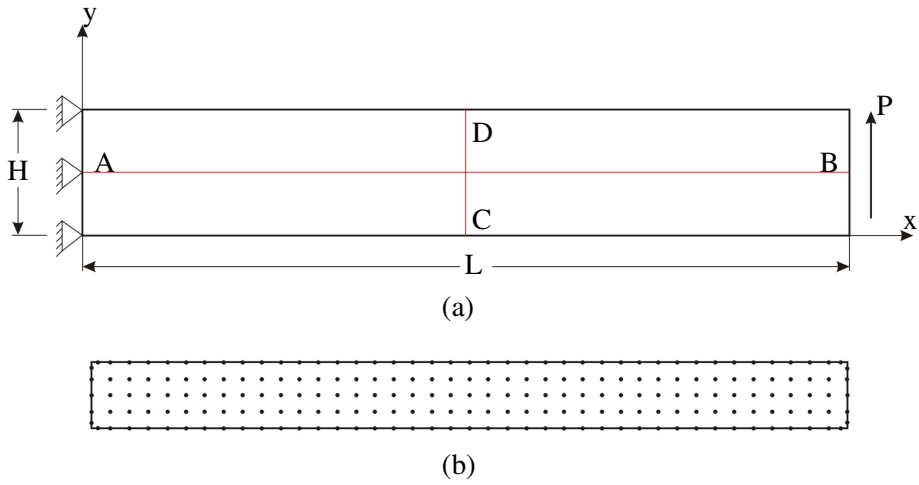
Figure 7: (a) Cantilever beam of L=10m and H=1m subjected to a bending loading. (b) Distribution of the used nodal points.
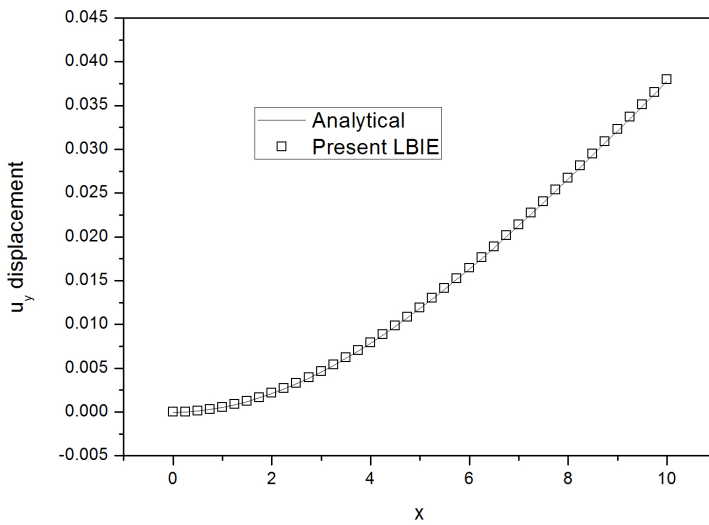
Figure 8: Vertical displacements across the line AB shown in Fig. 7(a).
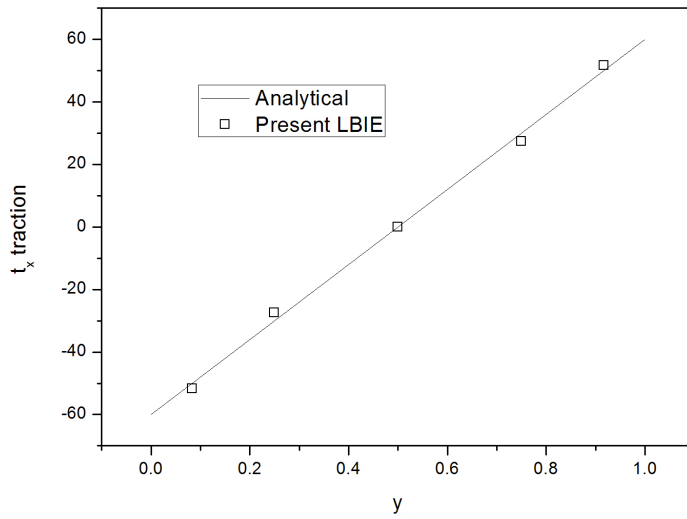
Figure 9: Axial tractions across the clamped side of the beam of Fig. 7.
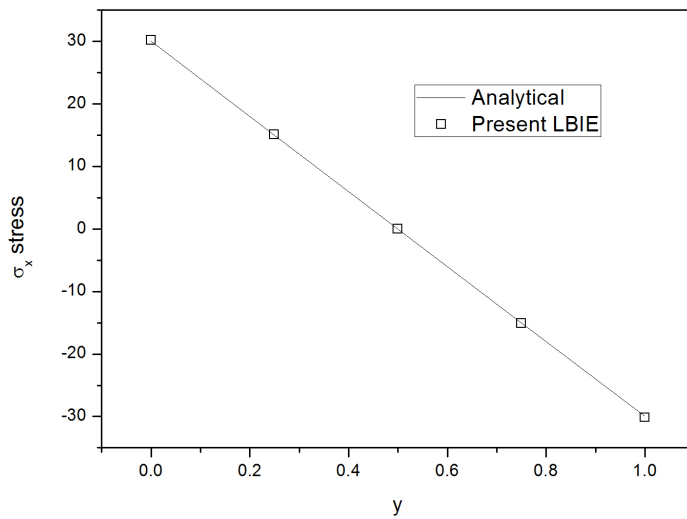
Figure 10: σ_x stress along the line CD of the beam of Fig. 7
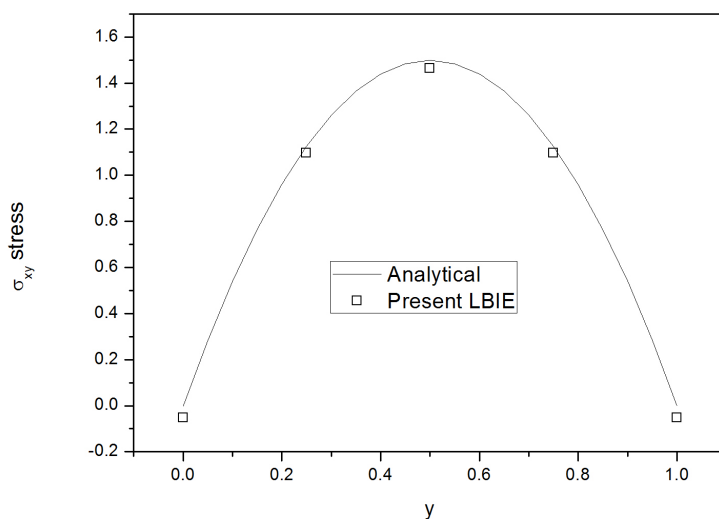
Figure 11: σ_{xy} stress along the line CD of the beam of Fig. 7

points with support domains of radius 0.37733 is employed. The horizontal displacements, the vertical tractions and the stresses σ_{rr}, $\sigma_{\theta\theta}$ at the side $\theta = 0$ have been evaluated and compared to the corresponding analytical solutions [Polyzos, Tsinopoulos, and Beskos (1998)] in Fig. 13, Fig. 14, Fig. 15 and Fig. 16, respectively. As it is apparent, the agreement between numerical and analytical results is very good.

5.4   Rectangular perforated plate in tension

The present benchmark problem deals with a $60m$x$60m$ plate with a circular hole of radius $a = 1$ at its center, subjected to a uniform tensile load $P = 1N/m^2$. The material properties are assumed to be $E = 100000N/m^2$ and $v = 0.25$ and due to the symmetry of the problem only the upper right quadrant of the plate is analyzed (Fig. 17(a)). For the solution of that problem 150 non-uniformly distributed points are considered (Fig. 17(b)) with their support domains defined in such a way so the well-defined integration star [Liszka, Duarte, and Tworzydlo (1996)] to be satisfied. The exact solutions for displacement and stresses in polar coordinates are provided in [Timoshenko and Goodier (1970)]. Fig. 18 and Fig. 19 demonstrates displacements ux and uy at the sides corresponding to polar angle $\theta = 0^o$ and $\theta = 90^o$,
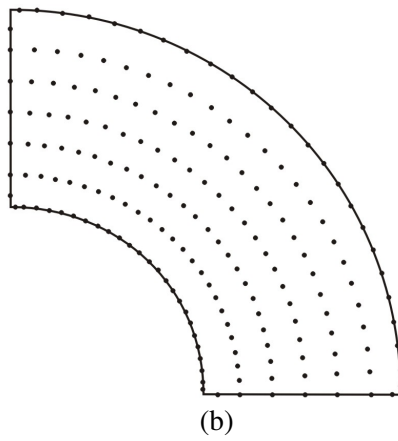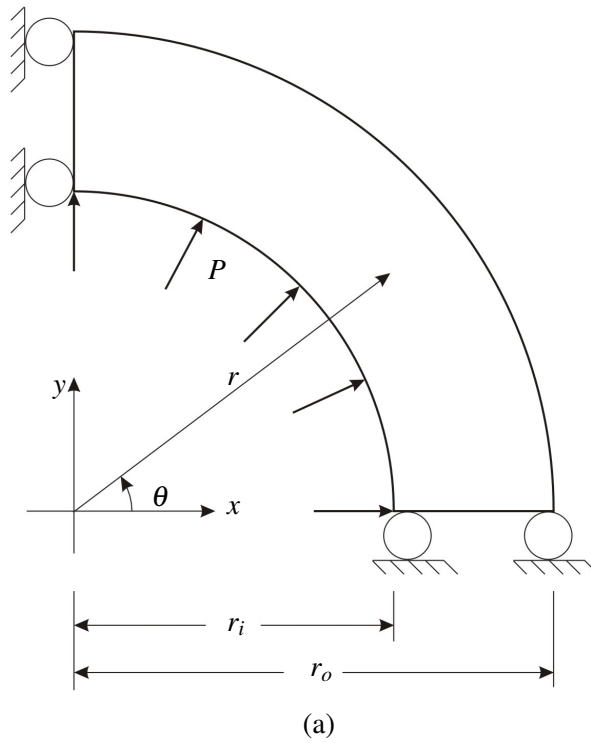
Figure 12: (a) One quarter of a cylindrical shell subjected to a uniform internal pressure. (b) Distribution of the used nodal points.
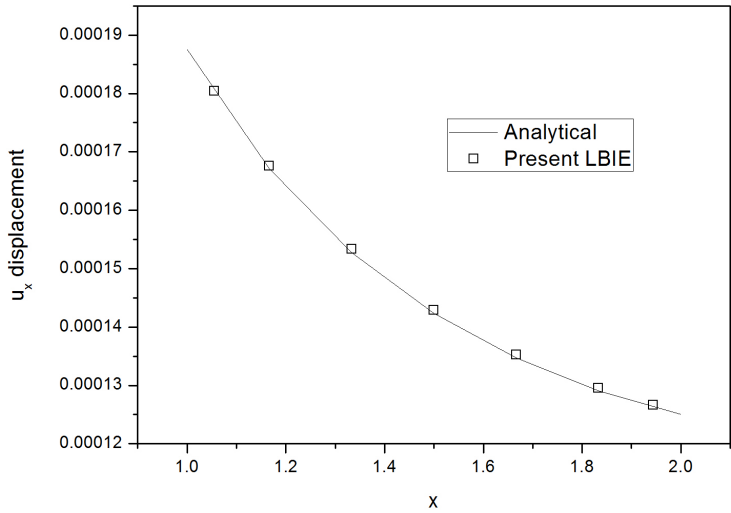
Figure 13: Horizontal displacements across the line $\theta = 0$ for the problem depicted in Fig. 12
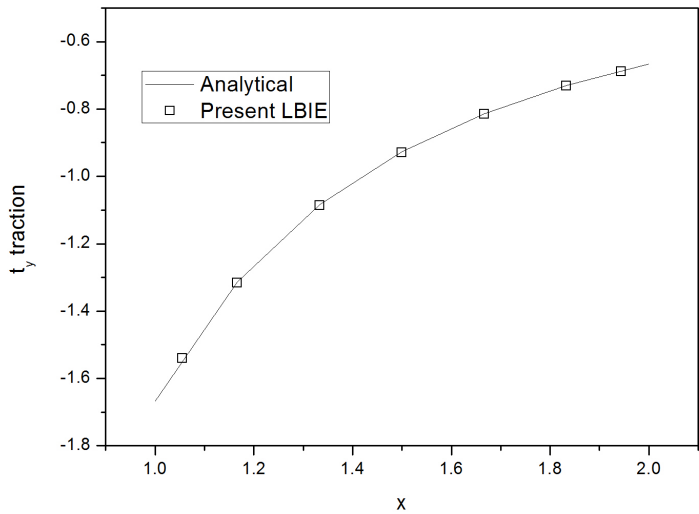
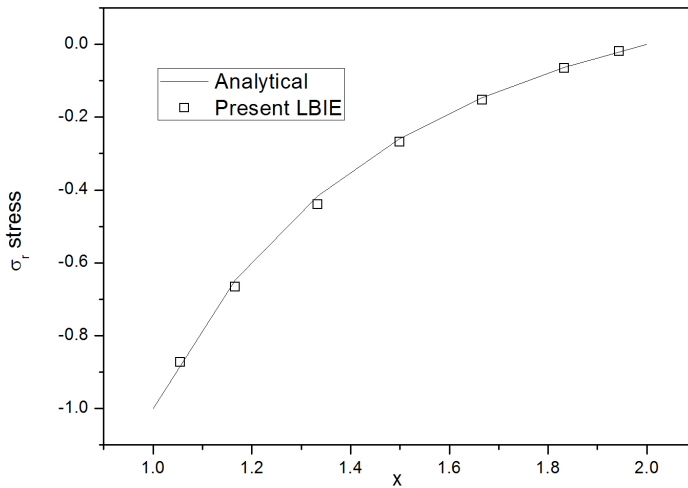Figure 14: Vertical tractions across the line $\theta = 0$ for the problem depicted in Fig. 12

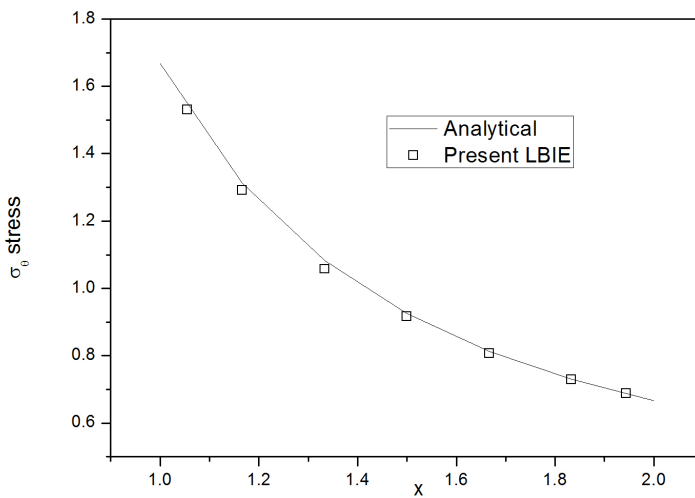Figure 15: σ_r stress along the line $\theta = 0$ for the problem depicted in Fig. 12

Figure 16: σ_θ stress along the line $\theta = 0$ for the problem depicted in Fig. 12

respectively, while Fig. 20 depicts the traction component t_y along the side with $\theta = 0^o$. Finally, Fig. 21, Fig. 22, Fig. 23 and Fig. 24 show stresses s_θ and σ_r at the sides corresponding to polar angle $\theta = 0^o$ and $\theta = 90^0$, respectively. All the obtained results are compared to analytical ones and as it is evident from the figures the achieved accuracy is very good.

5.5   *Rectangular inclusion subjected to a uniform pressure*

This example has been taken by the book of [Katsikadelis (2002)] and it is referred to a rectangular pipe subjected to a uniform internal pressure $p = 1MPa$. All the dimensions, the geometry and the boundary conditions of the problem are provided in Fig. 25. The material properties for the host medium are $E = 2x10^5 \ kN/m^2$ and $v = 0.20$, while 592 nodal points have been used for the solution of the problem. Fig. 26 demonstrates the tractions t_y along the line $y = 0$, while Fig. 27 and Fig. 28 present the distribution of stresses σ_x along the lines $y = 0$ and $y = 1.5m$, respectively. The obtained results are compared to the corresponding ones taken by the BEM package [ISoBEM (2012)]. With an exception to stresses σ_x across the line $y = 0$, the agreement of the results taken by the two methods is very good.

5.6   *Plate with an elliptical hole*

The last benchmark problem concerns a $800mm$x$800mm$ plate with an elliptical hole, subjected to a uniform tensile load $P = 100MPa$ as it is shown in Fig. 29. The two hemi-axis of the elliptical hole are $a = 8mm$ and $b = 2mm$, while the material properties of the plate are assumed to be $E = 3x10^6MPa$ and $v = 0.3$. For the solution of the problem 5176 nodal points are considered with their support domains defined as in previous benchmark problems. The obtained results are compared to the corresponding ones taken by the BEM package [ISoBEM (2012)]. Fig. 30-Fig. 33 portray the distribution of stresses σ_x and σ_y along the lines AB and CD (Fig. 29), respectively. From those figures it is apparent that the agreement between LBIE and BEM solutions is excellent.

6   Conclusions

A new meshless local boundary integral equation (LBIE) method for solving two-dimensional elastic problems has been proposed. Randomly distributed points without any connectivity requirement cover the analyzed domain and Local Radial Basis Functions (LRBFs) are employed for the meshless interpolation of displacements in the interior domain. The boundary of the considered elastic medium is represented via a mesh consisting of quadratic linear elements like those used in the Boundary Element Method (BEM). On the global boundary, displacements and
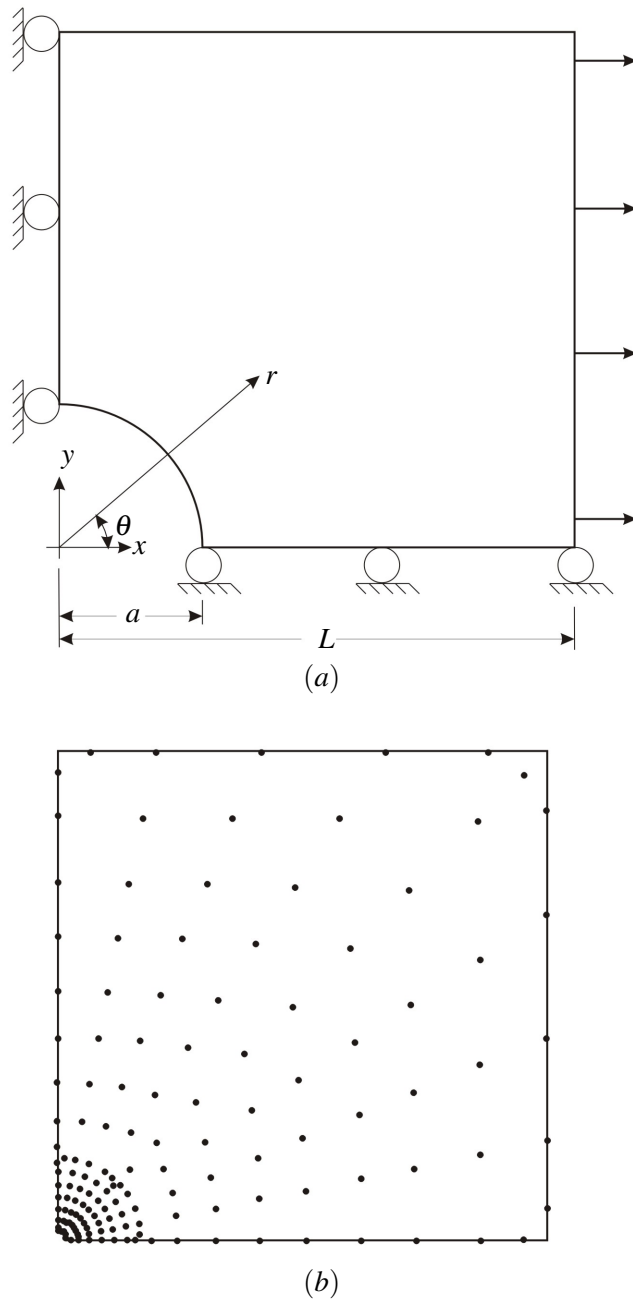
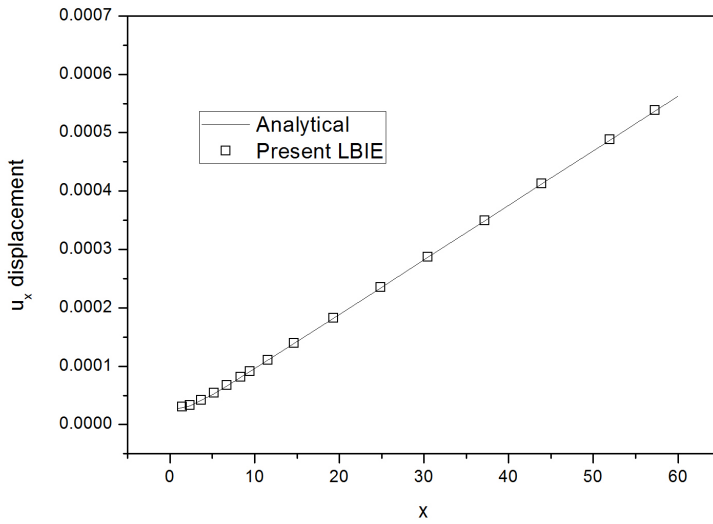Figure 17: (a) Perforated plate under tension, (b) discretization of the plate

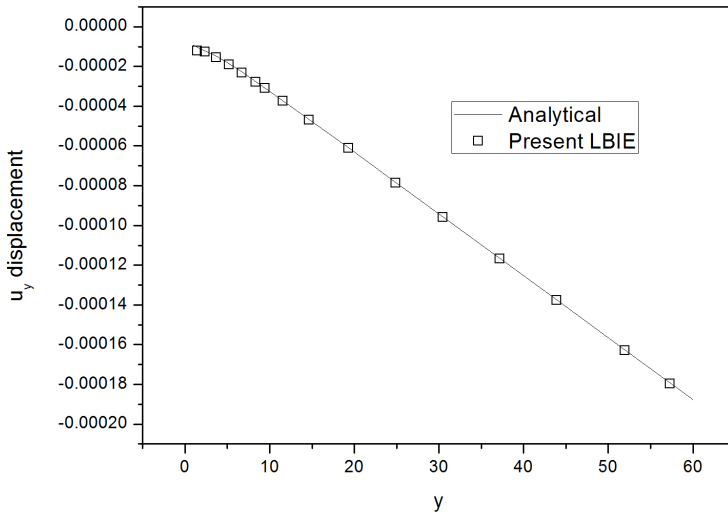Figure 18: u_x displacement along the side $\theta = 0$ of the plate of Fig. 17

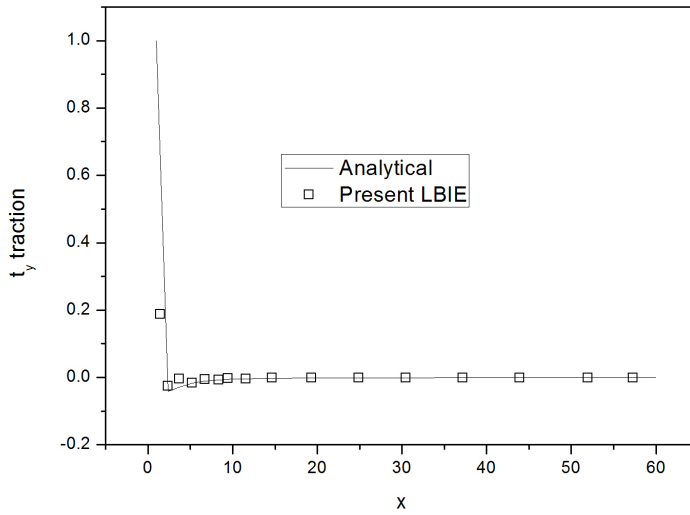Figure 19: u_y displacement along the side $\theta = 90^o$ of the plate of Fig. 17

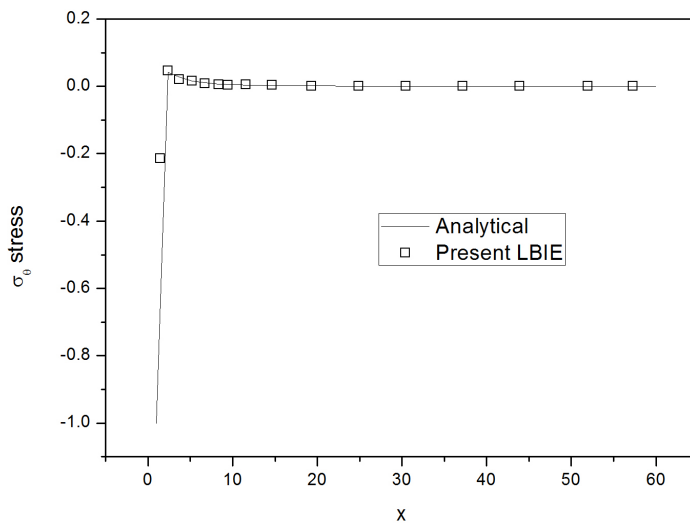Figure 20: t_y traction along the side $\theta = 0$ of the plate of Fig. 17

Figure 21: σ_θ stress component along the side $\theta = 0$ of the plate of Fig. 17
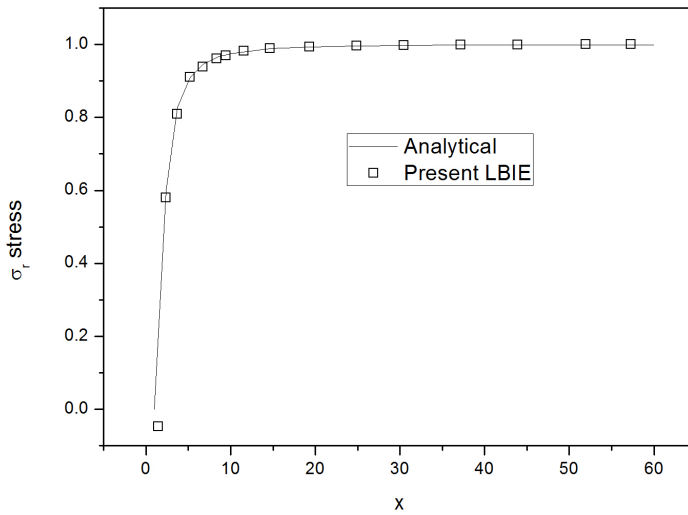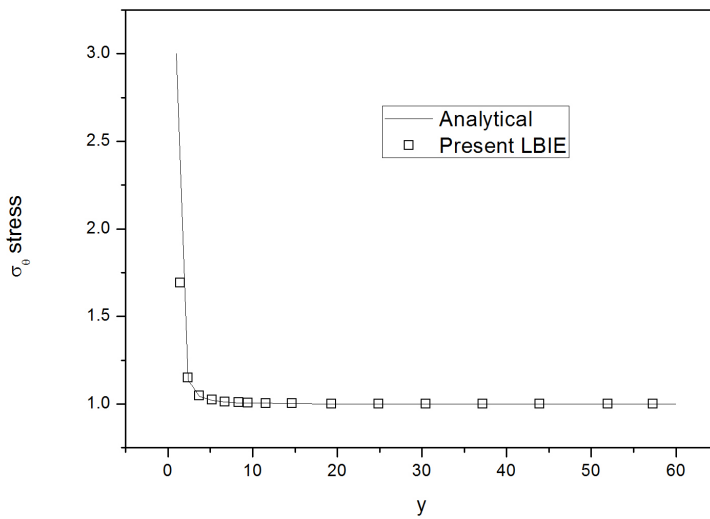
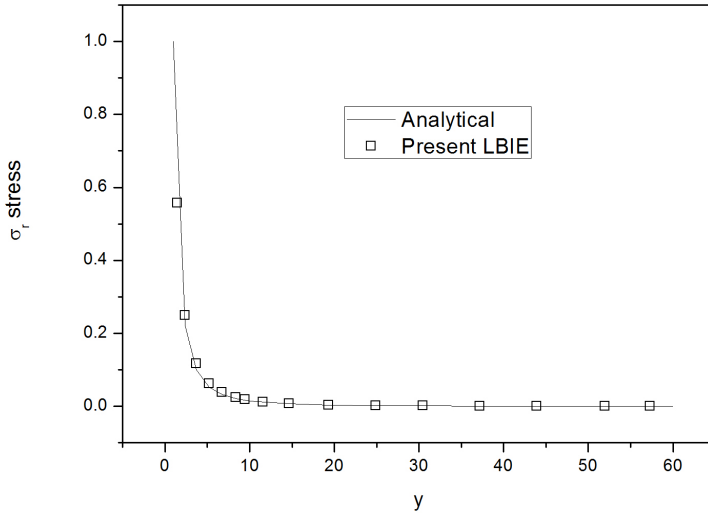Figure 22: σ_r stress component along the side $\theta = 0$ of the plate of Fig. 17

Figure 23: σ_θ stress component along the side $\theta = 90^o$ of the plate of Fig. 17

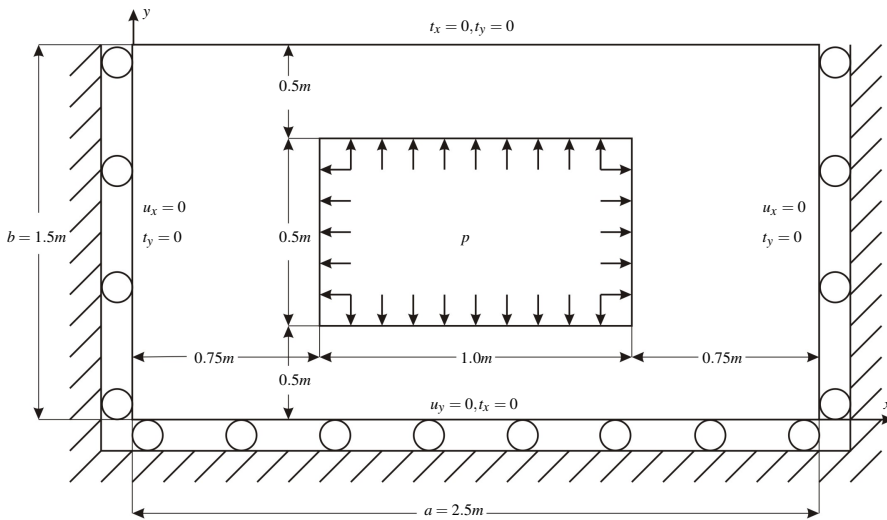Figure 24: σ_r stress component along the side $\theta = 90^o$ of the plate of Fig. 17

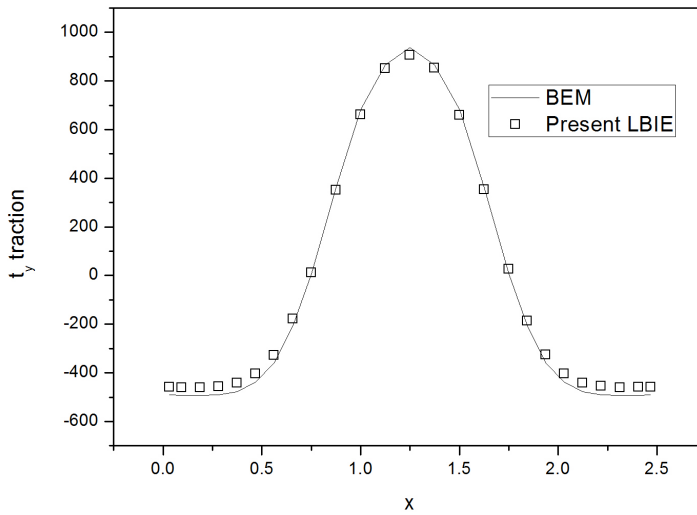Figure 25: The plane strain representation of a rectangular pipe subjected to a uniform pressure.

Figure 26: Distribution of tractions t_y along the boundary $y = 0$, for the problem of Fig. 25.
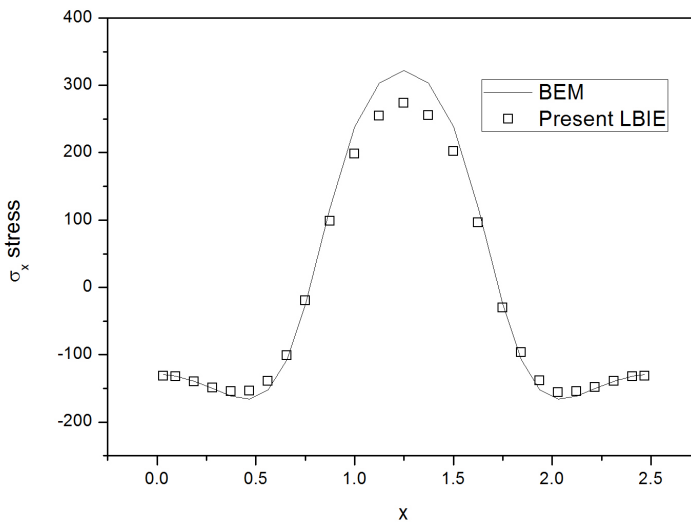

Figure 27: Distribution of stresses σ_x along the boundary $y = 0$, of the problem of Fig. 25.
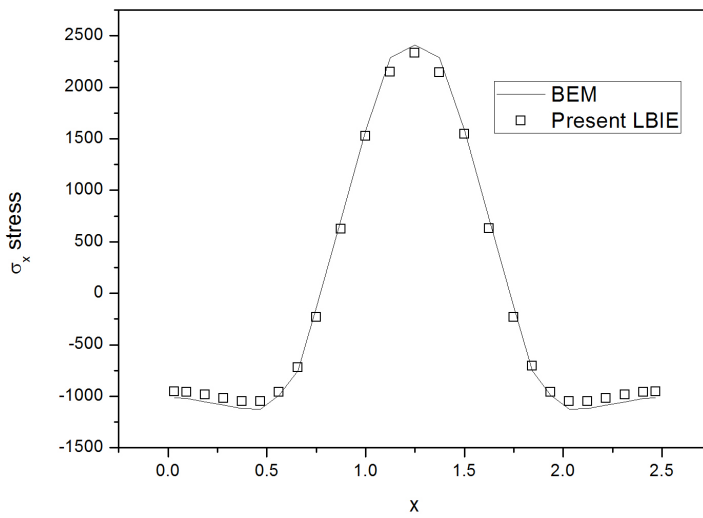
Figure 28: Distribution of stresses σ_x along the boundary $y = 1.5$ of the problem of Fig. 25.
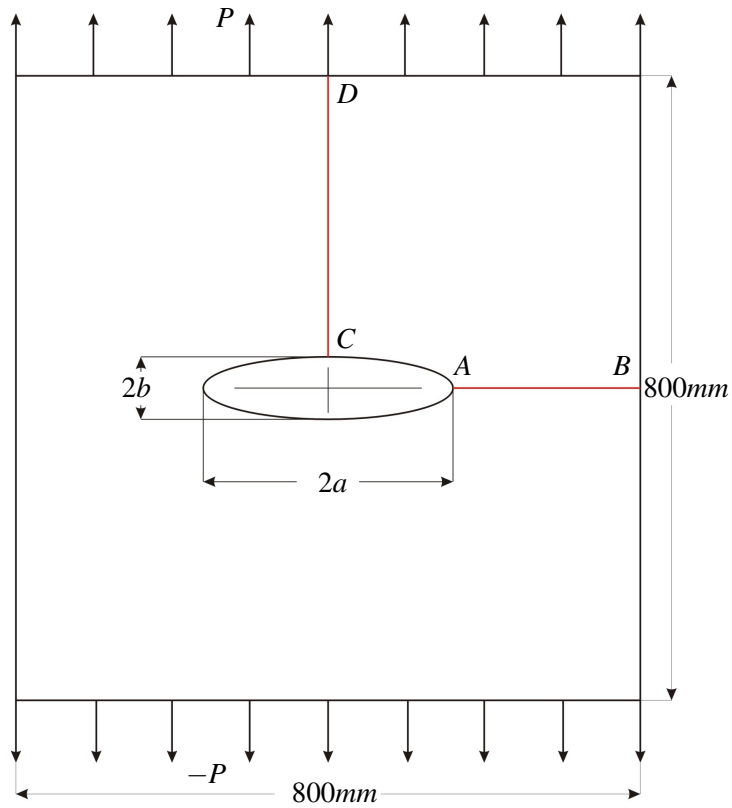
Figure 29: A square plate with an elliptical hole subjected to tensile stress
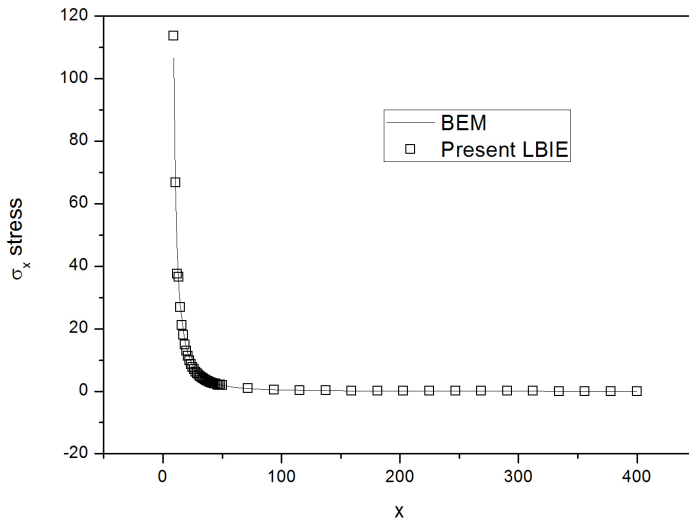
Figure 30: Distribution of stresses σ_x along the AB line of Fig. 29
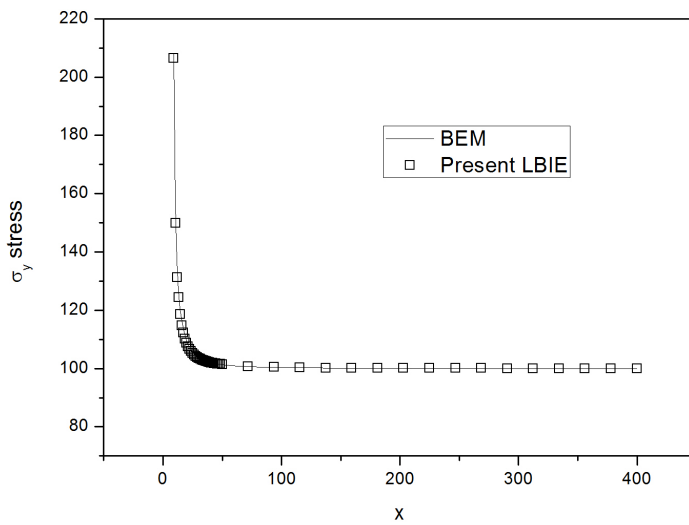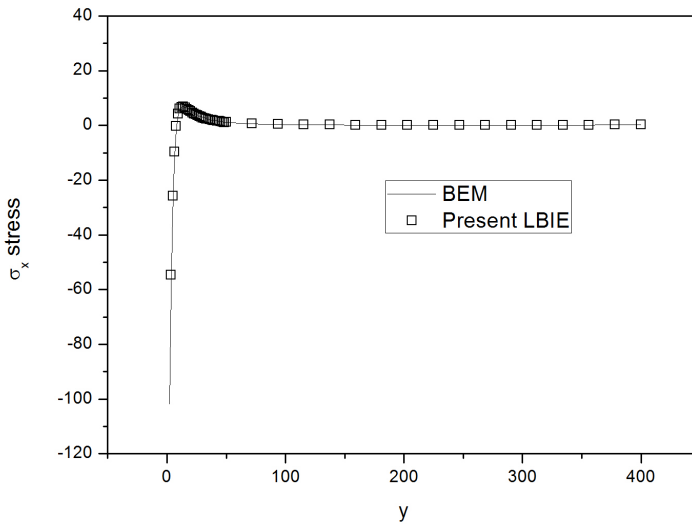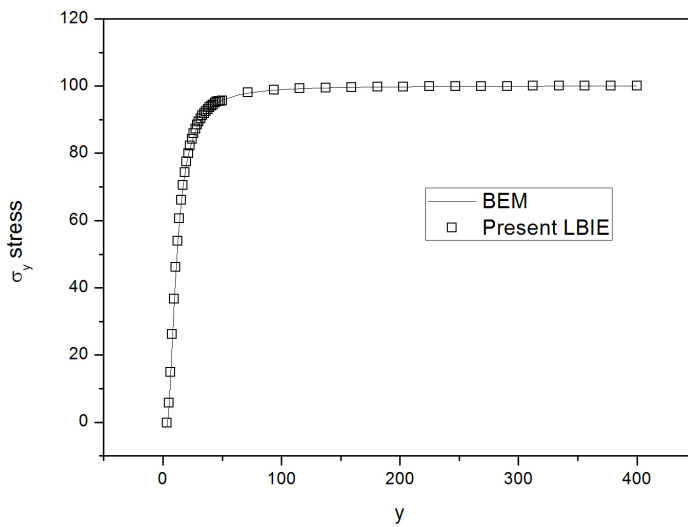

Figure 31: Distribution of stresses σ_y along the AB line of Fig. 29

Figure 32: Distribution of stresses σ_x along the CD line of Fig. 29

Figure 33: Distribution of stresses σ_y along the CD line of Fig. 29

tractions are treated as independed parameters of the problem. For each internal nodal point a circular support domain is centered and LBIEs for displacements and stresses are considered. At the local circular boundaries, the tractions involved in the aforementioned LBIEs are eliminated with the aid of properly defined companion solutions. All the integrations at local boundaries are performed quickly and economically with the aid of simple BEM-type integration techniques while all the fields are interpolated via RBFs after integrations. Six benchmark problems have been solved and the obtained results reveal the high accuracy of the method. The most important features of the proposed LBIE/RBF technique are its simplicity and efficiency as well as the fact that its extension to three dimensional problems is straightforward.

References

Agnantiaris, J.; Polyzos, D.; Beskos, D. (1996):   Some Studies on Dual Reciprocity BEM for Elastodynamic Analysis. *Computational Mechanics*, vol. 17, pp. 270–277.

Atluri, S. N. (2004):   *The Meshless Local Petrov-Galerkin (MLPG) Method*. Tech. Science Press.

Atluri, S. N.; Han, Z. D.; Shen, S. (2003):   Meshless local Petrov-Galerkin (MLPG) approaches for solving the weakly singular traction and displacement boundary integral equations. *CMES: Computer Modeling in Engineering & Sciences*, vol. 4, pp. 507–517.

Atluri, S. N.; Shen, S. P. (2002):   *The meshless local Petrov-Galerkin (MLPG) method*. Tech. Science Press.

Atluri, S. N.; Sladek, J.; Sladek, V.; Zhu, T. (2000):   The local boundary integral equation (LBIE) and its meshless implementation for linear elasticity. *Computational Mechanics*, vol. 25, pp. 180–198.

Bodin, A.; Ma, J.; Xin, X. J.; Krishnaswami, P. (2006):   A meshless integral method based on regularized boundary integral equation. *Computer Methods in Applied Mechanics and Engineering*, vol. 195, pp. 6258–6286.

Bourantas, G. C.; Skouras, E. D.; Loukopoulos, V. C.; Nikiforidis, G. C. (2010):   Numerical solution of non-isothermal fluid flows using Local Radial

Basis Functions (LRBF) interpolation and a velocity-correction method. *CMES: Computer Modeling in Engineering & Sciences*, vol. 64(2), pp. 187–212.

Gilhooley, D. F.; Xiao, J. R.; Batra, M. A.; McCarthy, M. A.; Gillespie, J. W. J. (2008): Two dimensional stress analysis of functional graded solids using the MLPG method with radial basis functions. *Computational Materials Science*, vol. 41, pp. 467–481.

Gosz, S.; Liu, W. K. (1996): Admissible approximations for essential boundary conditions in the reproducing kernel particle method. *Computational Mechanics*, vol. 19, pp. 120–135.

Han, Z. D.; Atluri, S. N. (2003): On simple formulations of weakly singular traction & displacement BIE, and their solutions through Petrov Galerkin approaches. *CMES: Computer Modeling in Engineering & Sciences*, vol. 4, pp. 5–20.

Han, Z. D.; Atluri, S. N. (2003): On Simple Formulations of Weakly-Singular Traction & Displacement BIE,and Their Solutions through Petrov-Galerkin Approaches. *CMES: Computer Modeling in Engineering & Sciences*, vol. 4, pp. 5–20.

Han, Z. D.; Atluri, S. N. (2007): A Systematic Approach for the Development of Weakly-Singular BIEs. *CMES: Computer Modeling in Engineering & Sciences*, vol. 21, pp. 41–52.

Hardy, R. L. (1990): Theory and applications of the multiquadrics-biharmonic method (20 years of discovery 1968–1988). *Computers and Mathematics with Applications*, vol. 19, pp. 163–208.

ISoBEM (2012): *BEM package*. www.bemsands.com.

Katsikadelis, J. T. (2002): *Boundary Elements: Theory and Applications*. Elsevier.

Liszka, T. J.; Duarte, C. A. M.; Tworzydlo, W. W. (1996): hp-Meshless cloud method. *Comp. Methods Appl. Mech. Engrg*, vol. 139, pp. 263–288.

Nardini, D.; Brebbia, C. (1982): A new approach to free vibration analysis using boundary elements. *In: Brebbia CA (ed) Boundary Element Methods in Engineering, Springer, Berlin*, vol. 50, pp. 313–326.

Okada, H.; Rajiyah, H.; Atluri, S. N. (1989): A Novel Displacement Gradient Boundary Element Method for Elastic Stress Analysis with High Accuracy. *J. Applied Mech.*, pp. 1–9.

Okada, H.; Rajiyah, H.; Atluri, S. N. (1989): Non-hyper-singular integral representations for velocity (displacement) gradients in elastic/plastic solids (small or finite deformations). *Comp. Mech.*, vol. 4, pp. 165–175.

Polyzos, D.; Tsinopoulos, S. V.; Beskos, D. E. (1998): Static and dynamic boundary element analysis in incompressible linear elasticity. *European. J. Mech. A/Solids*, vol. 17, pp. 515–536.

Saad, M. H. (2005): *Elasticity: Theory, Applications and Numerics*. Elsevier Butterworth-Heinemann.

Sellountos, E. J.; Polyzos, D. (2003): A MLPG (LBIE) method for solving frequency domain elastic problems. *CMES: Computer Modelling in Engineering & Sciences*, vol. 4, pp. 619–636.

Sellountos, E. J.; Polyzos, D. (2005): A meshless local boundary integral equation method for solving transient elastodynamic problems. *Computational Mechanics*, vol. 35 (4), pp. 265–276.

Sellountos, E. J.; Polyzos, D. (2005): A MLPG (LBIE) approach in combination with BEM. *Computer Methods in Applied Mechanics and Engineering*, vol. 194, pp. 859–875.

Sellountos, E. J.; Sequeira, A. (2008a): An advanced meshless LBIE/RBF method for solving two-dimensional incompressible fluid flows. *Computational Mechanics*, vol. 41, pp. 617–631.

Sellountos, E. J.; Sequeira, A. (2008b): A HybridMulti-Region BEM / LBIE-RBF Velocity-Vorticity Scheme for the Two-Dimensional Navier-Stokes Equations. *CMES: Computer Modelling in Engineering & Sciences*, vol. 23, pp. 127–147.

Sellountos, E. J.; Sequeira, A.; Polyzos, D. (2009): Elastic transient analysis with MLPG(LBIE) method and local RBFs. *CMES: Computer Modelling in Engineering & Sciences*, vol. 41, pp. 215–242.

Sellountos, E. J.; Sequeira, A.; Polyzos, D. (2010): Solving Elastic Problems with Local Boundary Integral Equations (LBIE) and Radial Basis Functions (RBF) Cells. *CMES: Computer Modelling in Engineering & Sciences*, vol. 57, pp. 109–135.

Sellountos, E. J.; Vavourakis, V.; Polyzos, D. (2005): A new Singular/Hypersingular MLPG (LBIE) method for 2D elastostatics. *CMES: Computer Modeling in Engineering & Sciences*, vol. 7 (1), pp. 35–48.

Selvadurai, A. P. S. (2000): *Partial Differential Equations in Mechanics 2*. Springer-Verlang, Berlin, Heidelberg.

Sladek, J.; Sladek, V. (2010): Local integral equations implemented by MLS-approximation and analytical integrations. *Engineering Analysis with Boundary Elements*, vol. 34, pp. 904–913.

Sladek, J.; Sladek, V.; Atluri, S. N. (2002):   Application of the local boundary integral equation method to boundary value problems.   *International Journal of Applied Mechanics*, vol. 38, pp. 1025–1043.

Sladek, J.; Sladek, V.; Keer, R. V. V. (2000):   Numerical integration of singularities of local boundary integral equations.   *Computational Mechanics*, vol. 25, pp. 394–403.

Sladek, J.; Sladek, V.; Keer, R. V. V. (2003):   Meshless local boundary integral equation method for 2D elastodynamic problems.   *International Journal of Numerical Methods in Engineering*, vol. 57, pp. 235–249.

Sladek, J.; Sladek, V.; Solek, P.; Tan, C. L.; Zhang, C. (2009):   Two and three dimensional thermoelastic analysis by the MLPG method.   *CMES: Computer Modelling in Engineering & Sciences*, vol. 47, pp. 61–96.

Timoshenko, S. P.; Goodier, J. N. (1970):   *Theory of Elasticity*.   McGraw-Hill 3rd Edition, New York.

Vavourakis, V. (2008):   A local hypersingular integral equation method using triangular background mesh.   *CMES: Computer Modelling in Engineering & Sciences*, vol. 36, pp. 119–146.

Vavourakis, V. (2009):   A meshless local boundary integral equation method for two-dimensional steady elliptic problems.   *Computational Mechanics*, vol. 44, pp. 777–790.

Vavourakis, V.; Polyzos, D. (2007):   A new MLPG(LBIE) method for solving 2D elastostatic problems.   *Computers Materials and Continua*, vol. 5 (3), pp. 185–196.

Vavourakis, V.; Polyzos, D. (2008):   A MLPG(LBIE) numerical method for solving 2D incompressible and nearly incompressible elastostatic problems.   *Communications in Numerical Methods in Engineering*, vol. 24, pp. 281–296.

Vavourakis, V.; Protopappas, V. I. C.; Fotiadis, D.; Polyzos, D. (2009):   Numerical determination of modal dispersion and AE signals characterization in waveguides through LBIE/BEM and time-frequency analysis.   *Computational Mechanics*, vol. 43, pp. 431–441.

Vavourakis, V.; Sellountos, E. J.; Polyzos, D. (2006):   A comparison study on different MLPG(LBIE) formulations.   *CMES: Computer Modeling in Engineering & Sciences*, vol. 13, pp. 171–184.

Wang, J. G.; Liu, G. R. (2002):   A point interpolation meshless method based on radial basis functions.   *International Journal of Numerical Methods in Engineering*, vol. 54 (11), pp. 1623–1648.

Wang, J. G.; Liu, G. R. (2002): On the optimal shape parameters of radial basis functions used for 2-D meshless methods. *Computer Methods in Applied Mechanics and Engineering*, vol. 191, pp. 2611–2630.

Wen, P. H.; Aliabadi, M. H. (2012): Analytical formulation of meshless local integral equation method. *Applied Mathematical Modelling*, vol. http://dx.doi.org/10.1016/j.apm.2012.05.006.

Zhu, T.; Zhang, J.; Wang, D. (2007): A meshless Local Petrov-Galerkin (MLPG) approach based on the regular local boundary integral equation for linear elasticity. *Int. J. Comput. Methods in Enng Sci. and Mechanics*, vol. 8, pp. 373–382.

Zhu, T.; Zhang, J. D.; Atluri, S. N. (1998): A local boundary integral equation (LBIE) method in computational mechanics and a meshless discretization approach. *Computational Mechanics*, vol. 21, pp. 223–235.